Chinese Chemical Letters 34 (2023) 107491

Contents lists available at ScienceDirect

Chinese Chemical Letters

journal homepage: www.elsevier.com/locate/cclet

Au/Ag_2S dimeric nanostructures for highly specific plasmonic sensing of mercury(II)

Xinyi Liang[a], Xu Du[a], Ao Liu[a], Zhixiong Cai[b], Jingwen Li[a], Maosheng Zhang[b], Qingxiang Wang[b,*], Jingbin Zeng[a,*]

[a] College of Chemistry and Chemical Engineering and State Key Laboratory of Heavy Oil Processing, China University of Petroleum (East China), Qingdao 266580, China
[b] College of Chemistry and Environment, Fujian Provincial Key Laboratory of Modern Analytical Science and Separation Technology, Minnan Normal University, Zhangzhou 363000, China

ARTICLE INFO

Article history:
Received 15 January 2022
Revised 16 April 2022
Accepted 5 May 2022
Available online 10 May 2022

Keywords:
Au/Ag_2S dimeric nanoparticles
Mercury ion
Colorimetric detection
High selectivity

ABSTRACT

Although many plasmonic nanosenosrs have been established for the detection of mercury(II) (Hg^{2+}), few of them is feasible for analyzing natural samples with very complex matrices because of insufficient method selectivity. To address this challenge, we propose an epitaxial and lattice-mismatch approach to the synthesis of a unique Au/Ag_2S dimeric nanostructure, which consists of an Au segment with excellent plasmonic characteristics, and a highly stable Ag_2S portion with minimum solubility product ($K_{sp}(Ag_2S) = 6.3 \times 10^{-50}$). The detection relies on the chemical conversion of Ag_2S to HgS when reacting with Hg^{2+}, resulting in a red shift in the absorption band of the connecting Au NPs. The concurrent color changes of the solution from gray purple to dark green and finally to navy correlate well with Hg^{2+} concentration, thus enables UV–vis quantitation and a naked-eye readout of the Hg^{2+} concentration. This method exhibits superior selectivity towards Hg^{2+} over other interfering ions tested because Hg^{2+} is the only ion that can react with Ag_2S to form HgS with even smaller solubility product ($K_{sp}(HgS) = 4 \times 10^{-53}$). The detection limit of this method is 1.21 μmol/L, calculated by the signal-to-noise of 3. The practicability of the method was verified by analyzing the Hg^{2+} in sewage water samples without sample pretreatment with satisfactory recoveries (93.1%-102.8%) and relative standard deviations (1.38%-2.89%). We believe this method holds great potential for on-the-spot detection of Hg^{2+} in environmental water samples with complex matrices.

Environmental pollution and diseases caused by heavy metals and their compounds have been one of the major global public health concerns, especially mercury pollution [1–3]. Mercury is a highly toxic pollutant, which can get into the body *via* skin contact or diet and destroy the human central nervous system, immune system, kidney function, *etc*. In the meantime, it can be enriched and amplified in organisms through food chain [4,5]. Hence the detection of the mercury content in environment is necessary for protecting human health.

Conventional approaches for the detection of Hg^{2+} include atomic absorption spectrometry [6], atomic fluorescence spectroscopy [7–9], inductively coupled plasma mass spectrometry (ICP-MS) [10], and inductively coupled plasma atomic emission spectrometry (ICP-AES) [11], *etc*. These methods are always sensitive and selective, and can satisfy the qualitative or quantitative detection of mercury. However, most of them require costly and cumbersome instruments, skilled technicians, and time-consuming pretreatment processes, which greatly limits their application in real-time and on-site detection.

Colorimetry has found broad application for on-the-spot detection of a wide range of analytes, because of its simple operation, visual readout and low instrument requirements [12]. In addition to organic dyes applied in conventional colorimetric approaches, plasmonic nanoparticles (NPs) have been widely designed as nanoprobes for colorimetric sensing, as a result of their tunable localized surface plasmon resonance (LSPR) effects [13]. The intensity and frequency of LSPR are strongly associated with the size, composition, morphology, the dielectric properties of the nanoparticles, and dielectric environment, which offers an opportunity to design specific nanoprobes for target analytes [14]. A common strategy is utilizing the analyte-induced assembly and dispersion of nanoparticles, which always require ligand modifica-

* Corresponding authors.
E-mail addresses: axiang236@vip.163.com (Q. Wang), xmuzjb@163.com (J. Zeng).

https://doi.org/10.1016/j.cclet.2022.05.005
1001-8417/

tion that can form hydrogen bonds, metal-ligand complexes, *etc.* For example, a series of ligands containing thiols [15–17], DNA [18,19], peptides [20,21], proteins [22] and others [23,24] have been modified onto the surface of plasmonic nanoparticles to develop Hg^{2+} nanosensors. These methods often require additional ligand synthesis, and most of them have insufficient selectivity making it difficult for the detection of Hg^{2+} in natural samples with complex matrices.

Janus nanoparticles are a special class of particles with asymmetric structures and compositions. The two sides of nanoparticles have different properties, resulting in interface electron transfer and synergistic effects. They have found extensive applications in biomedicine [25], catalysis [26], biosensing [27], and other fields. Among numerous Janus nanoparticles, bimetallic nanoparticles with noble metal (Au and Ag) or metallide at its dimeric structure are considered to be ideal candidates as colorimetric nanoprobes, because their two active centers are both exposed, and their LSPR effect is more sensitive to the changes in morphology, size, composition and other properties [28]. Thus, engineering bimetallic nanoparticles with desirable dimeric structures is supposed to be essential for improving the sensitivity and selectivity of colorimetric method [28,29].

In this work, we attempted to develop a high-performance Hg^{2+} nanosensor by constructing an Au/Ag_2S dimeric structure, which is composed of an Au core with tunable LSPR effect, and an Ag_2S portion having exclusive response towards Hg^{2+}. Ag_2S is a stable and insoluble sulfide precipitate with minimum solubility product (K_{sp} (Ag_2S) = 6.3×10^{-50}), making it highly inert towards all anions. Theoretically, only Hg^{2+} can react with Ag_2S to form HgS (K_{sp} (HgS) = 4×10^{-53}). When Au/Ag_2S NPs are exposed to Hg^{2+}, Ag_2S will be transformed to HgS, leading to the changes in the composition of the shells, thereby changing the LSPR effect. So the color and absorption changes which are associated with the Hg^{2+} concentration can be observed by naked eyes or monitored by UV–vis spectroscopy (Fig. 1). Thus, a naked-eye readout and spectral quantitation for Hg^{2+} concentration can be obtained. The specificity of the method was validated by successfully analyzing raw sewage samples without any pretreatment.

Tetrachloroauric acid, trisodium citrate, silver nitrate, iodine, and all the other inorganic compounds were bought from Sinopharm Chemical Reagent Co., Ltd. The silver ammonia solution (0.03 mol/L) was obtained by blending $AgNO_3$ (0.1 mol/L, 6 mL), $NH_3 \cdot H_2O$ (25%–28%, 1240 μL), and NaOH (3 mol/L, 650 μL). Stock solution of $Hg(NO_3)_2$ (1000 mg/L) was provided by TanMo Quality Testing Technology Co., Ltd. (Beijing, China). Sewage and tap water samples were collected from a sewage disposal exit in our campus and the lab, respectively. Deionized water was used for all experiments. UV–vis spectra were acquired from a spectrophotometer (UV-2450, Shimadzu). Transmission electron microscopy (TEM) images were captured by a JEM 1400 microscope (JEOL). High-angle annular dark-field scanning transmission electron microscopy (HAADF-STEM), high-resolution transmission electron microscopy (HRTEM), and energy dispersive X-ray (EDX) elemental mapping measurements were conducted on a Tecnai F30 microscope. Powder X-ray diffraction (XRD) was measured by a X'Pert diffractometer (PANalytical).

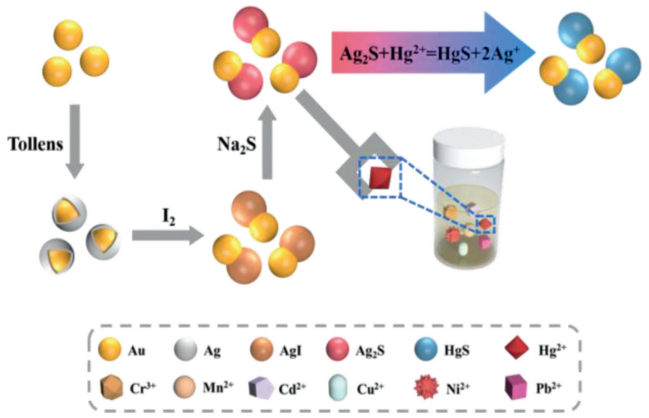

Fig. 1. Scheme of the method for the detection of Hg^{2+} using Au/Ag_2S dimeric NPs.

Citrate-stabilized Au NPs with the diameter of 13 nm were synthesized using a standard citrate method. Briefly, 10 mL of trisodium citrate (38.8 mmol/L) was injected into the boiling water (100 mL) containing 5 mL of $HAuCl_4$ (24.28 mmol/L). After heating for 15 min, the faint yellow solution turned wine-red, which suggested Au NPs (13-nm diameter) had been successfully synthesized. Then, using the pre-made Au NPs as seeds, Au@Ag core-shell NPs were prepared *via* the epitaxial deposition of Ag on Au surface. In brief, 13 nm Au NPs (2 mL) were added into the mixture containing silver ammonia solution (0.3 mL), formaldehyde (HCHO) (0.48 mL, 0.01 mol/L) and ultrapure water (7.22 mL) and stirred for 10 min at 25 °C. During the reaction, the colloid color gradually turned from wine-red to orange, suggesting the generation of Au@Ag core-shell NPs. To synthesize Au@Ag core-shell NPs which have different shell thicknesses, we can alter the ratio between HCHO and silver ammonia solution. Hence, we chose to fix the amount of HCHO, and adjusted the concentration of silver ammonia solution to alter the ratio. Afterwards, 0.5 mL of I_2 was titrated into Au@Ag core-shell NPs (4 mL) and the mixture was stirred for 5 min, during which the colloid color varied from orange to purple-red. By changing the amount of I_2, Au/AgI NPs with different AgI thickness were prepared to explore the influence on detection effect. Finally, Au/Ag_2S NPs were acquired *via* the mix of Na_2S (1.5 mL) and Au/AgI NPs (4.5 mL), whose color changed from purple-red to gray purple. After stirring for 10 min, a certain amount of PVP was added to reduce the risk of agglomeration. The supernatant was removed by centrifuging at 12,000 rpm for 10 min, redispersed in water. By varying Na_2S concentration, the thickness effect of Ag_2S on method sensitivity was studied.

The Hg^{2+} standard solutions of different concentrations in the range of 0–154 μmol/L were mixed with the prepared Au/Ag_2S NPs in a ratio of 1:9, and the UV–vis spectrophotometer was used for spectral determination. For assessing the practicability of Au/Ag_2S NPs for natural water sample analysis, recovery experiments were carried out for detecting tap water and sewage samples. Firstly, we determined the Hg^{2+} concentrations in water samples. Then, known amounts of Hg^{2+} at different concentrations (30.81, 61.61 and 77.02 μmol/L) were spiked into these samples. Each sample was tested three times. According to the working curve equation, the Hg^{2+} content in different samples was obtained, and then the recovery rate and relative standard deviation (RSD) were calculated to evaluate the practicability of the method. The recovery was calculated by the formula $R = (C_t\text{-}C_0)/C_s \times 100\%$, where C_t is the analytical result of the spiked sample, C_0 is the result before spiking of the sample, and C_s is the amount of constituent added to the sample.

Au NPs with a diameter of 13 nm were prepared by the standard citrate method, and then Ag shells were epitaxially grown onto the surface of Au NPs by silver mirror reaction. The uniform morphology could be observed on the basis of the analysis of the TEM image and the histogram of size distribution of Au@Ag core-shell NPs (Fig. S1 in Supporting information), and the average size is 21.3 ± 1.9 nm. After that, I_2 was added to oxidize the Ag shell to generate Au/AgI dimeric NPs. It can be seen from Figs. 2a and b that Au/AgI NPs have a dimeric structure, which consists of Au centers with dark contrast and AgI shells with light contrast. HAADF-STEM and EDX elemental maps were utilized to characterize the chemical components and distribution of nanoparticles. Figs. 2c-f

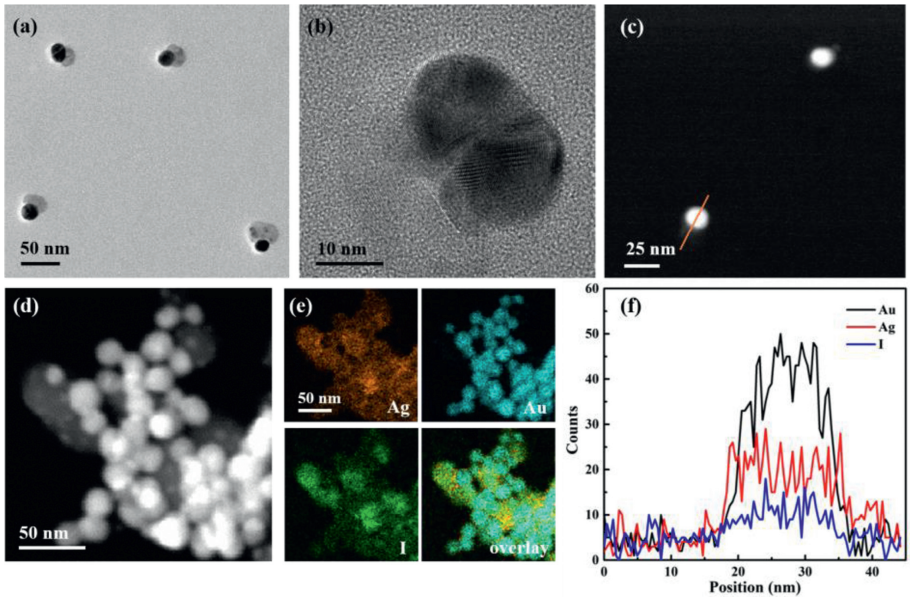

Fig. 2. (a) TEM image, (b) HRTEM image, (c, d) HAADF-STEM image, (e, f) EDX elemental maps of Au/AgI NPs. Orange line in (c) represents the EDX line scan shown in (f).

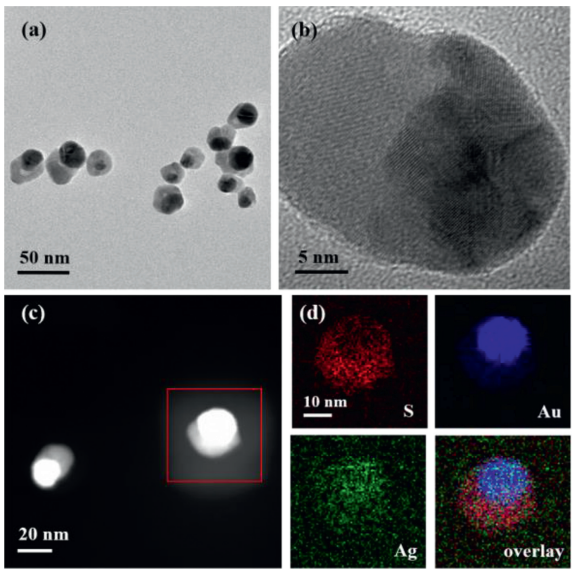

Fig. 3. (a) TEM image, (b) HRTEM image, (c) HAADF-STEM image, (d) EDX elemental maps of Au/Ag_2S NPs.

depict that Ag and I mostly overlap to form the AgI shell, and the shell mostly coated on the side of the Au core and only a thin layer on the other side, which further confirms the proposed dimeric structures. It is worth noting that AgI is susceptible to high voltages, making them easily decompose during the STEM test. Therefore, the mapping result shows partial aggregation. Such a dimeric nanostructure was formed due to the lattice-mismatch between Au and AgI as reported previously [28].

To obtain the Au/Ag_2S dimeric NPs, Na_2S was used to etch and precipitate AgI shell into Ag_2S. Typical TEM and HRTEM images in Figs. 3a and b illustrate that the resulting nanoparticles still maintain the dimeric structure, consisting of a dark Au core and an Ag_2S attachment. The HAADF-STEM image and the EDX elemental maps (Figs. 3c and d) further confirm that the generated nanoparticles have the dimeric structure and the Au primarily located in the core, while Ag_2S predominantly located at the side.

For revealing the colorimetric detection mechanism, the UV–vis spectra of the synthesized products in each step and the final detection products were characterized. As displayed in Fig. 4a, the LSPR band of Au NPs was centered at 520 nm and the solution was wine-red. Upon the addition of silver ammonia solution and HCHO, the absorption peak of sliver shell appeared at 392 nm, and the peak of Au blue-shifted from 520 nm to 494 nm due to the shielding effect by Ag [30]. Simultaneously, the colloid color turned to orange. Then, I_2 was added in, and the solution gradually varied from orange to purple-red. A new band appeared at 421 nm, and it can be regarded as the band gap absorption of AgI [31]. Simultaneously, the absorption band of Au returned to 521 nm again, indicating that the shielding effect of sliver shell was weakened owing to the formation of Au/AgI NPs. This is in accordance with the characterization results in Fig. 2. Following the addition of Na_2S to form Au/Ag_2S dimeric NPs, the solution turned gray purple and the LSPR band at 421 nm vanished while the band at 521 nm moved to 562 nm. Such a redshift alludes to the transformation from AgI to Ag_2S, giving rise to the enhancement in the refractive index of the media around the Au NPs [28,32-34]. When a certain concentration of Hg^{2+} was mixed with the nanoprobes, a color change from gray purple to dark green and finally to navy occurred and the peak redshifted to 569 nm. The red-shift of spectrum can be attributed to the transformation of the composition from Ag_2S to HgS with increasing refractive index from ~2.2 to ~2.9 [33–36].

To reveal the composition transformation, TEM and HAADF-STEM were utilized to characterize the nanoparticles generated from the reaction between Au/Ag_2S dimeric NPs and Hg^{2+}. Figs. 4b-d show that the generated products also possess a dimeric structure analogous to that of Au/Ag_2S NPs. By means of lattice fringe analysis, we found (111) HgS with lattice spacing of 3.4 Å and (111) Au with lattice spacing of 2.4 Å in a single particle. To further figure out their elemental distribution, EDX elemental mapping measurements were employed. According to Fig. 4e, it can be seen that Au, as the core of the nanostructure, has a regular spherical shape, while S and Hg are basically in the same position, which can be inferred to form HgS and accumulate on the side of the core. Fig. 4f shows that Hg and S appeared simultaneously before Au in the line scan direction. Thus, the shell layer was transformed from Ag_2S to HgS to form the Au/HgS dimeric NPs. In addition,

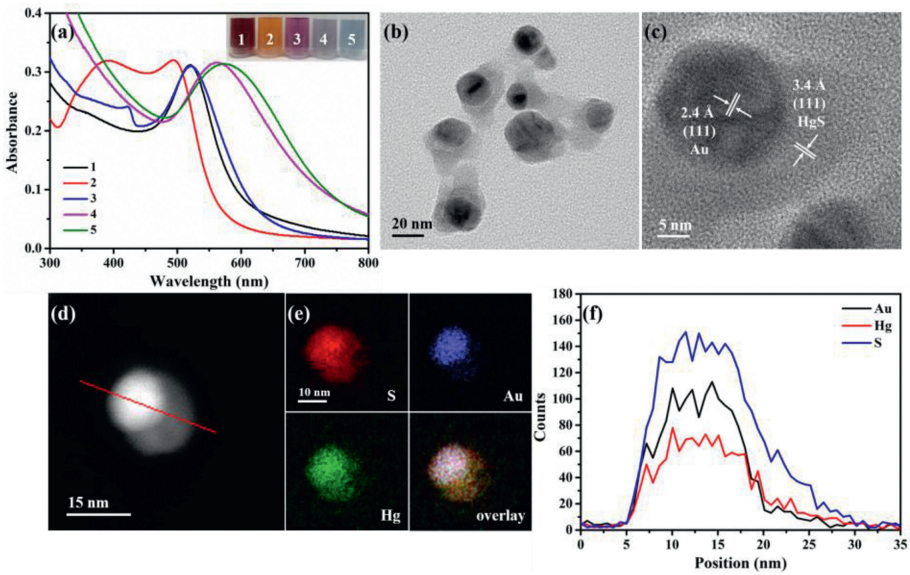

Fig. 4. (a) UV–vis spectra of Au NPs (1), Au@Ag NPs (2), Au/AgI NPs (3), Au/Ag_2S NPs (4), and Au/Ag_2S NPs + Hg^{2+} (5). The inset is photograph of corresponding solutions. (b) TEM image, (c) HRTEM image, (d) HAADF-STEM image, (e, f) EDX elemental maps of Au/Ag_2S NPs + Hg^{2+}. Red line in d represents the EDX line scan shown in (f).

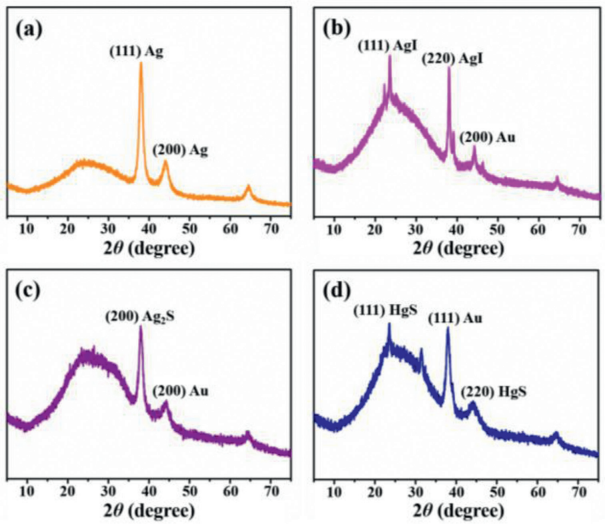

Fig. 5. XRD results of (a) Au@Ag NPs, (b) Au/AgI NPs, (c) Au/Ag_2S NPs, (d) Au/HgS NPs.

Fig. 5 presents the XRD results of Au@Ag core-shell NPs, Au/AgI dimeric NPs, Au/Ag_2S dimeric NPs, and Au/HgS dimeric NPs. These results validate the transformation of Ag, AgI, Ag_2S and HgS in order.

The above results elucidate that the colorimetric detection mechanism depends on the fact that Hg^{2+} can react with Ag_2S to constitute HgS, thereby varying the components and morphology of the nanomaterials and eliciting obvious spectral and color changes. The reaction between Au/Ag_2S dimeric NPs and Hg^{2+} is shown below:

$$Ag_2S + Hg^{2+} = HgS + 2Ag^+,\ K^0 = 1.575 \times 10^3 \quad (1)$$

On account of the low solubility product of Ag_2S, Au/Ag_2S NPs are resistant to reacting with most interfering compounds, suggesting the great feasibility and high specificity of the colorimetric method for Hg^{2+} detection.

On the basis of the above detection mechanism, the method sensitivity is highly relevant with the morphology and size of Au/Ag_2S NPs. In order to obtain high detection efficiency, the core-to-shell proportion of Au@Ag NPs, the amount of I_2 and the concentration of S^{2-} were optimized.

The concentration ratio between sliver ammonia solution and HCHO determines the core-to-shell proportion of Au@Ag NPs, which can further impact the shell thickness of Au/Ag_2S NPs. Herein, we fixed the concentration of HCHO (0.01 mol/L), and varied the concentration of $[Ag(NH_3)_2]^+$ from 0.06, 0.12, 0.24, 0.48, 0.72 to 0.96 mmol/L. When the concentration of $[Ag(NH_3)_2]^+$ was low, the generated Ag shell was thin and the final Ag_2S shell was also thin. After the addition of Hg^{2+}, the spectral changes were minor and the sensitivity was low (Fig. S2 in Supporting information). For comparison, when the $[Ag(NH_3)_2]^+$ with a higher concentration was added, a thicker Ag shell was generated, which had a greater shielding effect on the Au core. This led to a narrow range of spectral variations, which was also not conducive to visual observation and spectral analysis (Figs. S2c-f). Fig. S2b shows the resultant nanomaterials exhibited the highest sensitivity as the concentration of $[Ag(NH_3)_2]^+$ is 0.12 mmol/L.

Another crucial factor is the amount of I_2 because it impacts on the conversion efficiency of Ag to AgI. Au/AgI NPs acquired by different amounts of I_2 (0, 200, 500 and 700 μL) were used to form Au/Ag_2S NPs for Hg^{2+} detection. Figs. S3a and b (Supporting information) demonstrates that insufficient I_2 caused a narrow detection range of Hg^{2+} for the final synthetic Au/Ag_2S NPs. This is probable due to the fact that insufficient I_2 cannot completely oxidize Ag shell and the nanoparticles were still core-shell structure, which produced deficient Ag_2S shell for Hg^{2+} sensing. Excessive I_2 produced thick AgI shell, which had a strong shielding effect and reduced the synergistic effect, and compromised the sensitivity (Fig. S3d in Supporting information). Therefore, as displayed in Fig. S3c (Supporting information), we selected 500 μL I_2 to obtain the nanoprobes.

The influence of Ag_2S attachments thickness on detection effect was also explored by transforming AgI to Ag_2S with different S^{2-} concentration (0, 0.2, 0.5, and 0.7 mmol/L). Based on the results provided in Fig. S4 (Supporting information), a small amount of S^{2-} added caused inadequate conversion from AgI to Ag_2S and affected the detection of Hg^{2+}. While adding a large amount of S^{2-}, the spectrum become irregular. Finally, we chose 0.2 mmol/L Na_2S to synthesize Au/Ag_2S NPs for Hg^{2+} detection.

Table 1
Analysis of Hg^{2+} in natural water samples.

Water Samples	Detected (μmol/L)	Spiked (μmol/L)	Found (μmol/L)	Recovery (%)	RSD (%)
Tap water	0	30.81	30.96	100.5	2.56
		77.02	79.14	102.8	2.89
Sewage	15.40	30.81	43.01	93.1	2.28
		61.61	74.95	97.3	1.38

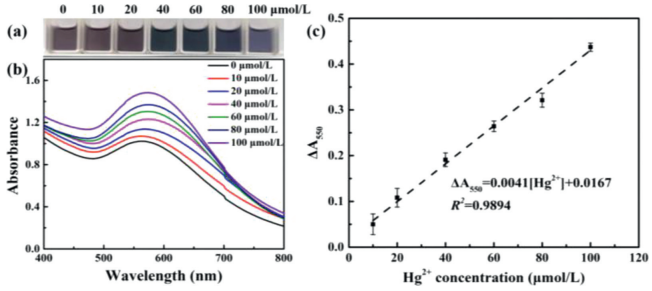

Fig. 6. (a) Photographs and (b) UV–vis spectra of Au/Ag_2S NPs reacting with various Hg^{2+} concentrations. (c) The linear relationship between decreased absorbance at 550 nm and Hg^{2+} concentrations.

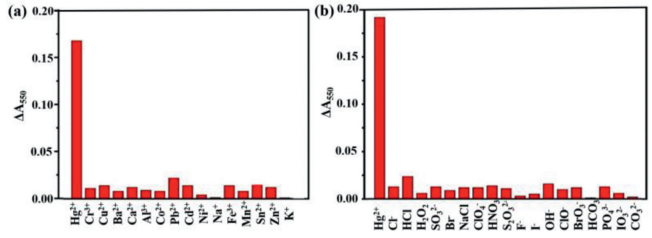

Fig. 7. The ΔA_{550} of Au/Ag_2S NPs reacting with Hg^{2+} or interfering compounds (K^+, Na^+, 30 mmol/L; Ca^{2+}, Zn^{2+}, Ba^{2+}, Cd^{2+}, Cu^{2+}, Sn^{2+}, Ni^{2+}, Mn^{2+}, Co^{2+}, 2 mmol/L; Cr^{3+}, Pb^{2+}, Al^{3+}, 1.5 mmol/L; Fe^{3+}, 1 mmol/L) (a) and (NaCl, Cl^-, HCO_3^-, CO_3^{2-}, 50 mmol/L; HCl, HNO_3, H_2O_2, IO_3^{2-}, Br^-, I^-, OH^-, 25 mmol/L; ClO^-, F^-, PO_4^{3-}, ClO_4^-, $S_2O_3^{2-}$, 12.5 mmol/L; SO_3^{2-}, BrO_3^-, 5 mmol/L) (b).

The performance of the developed method including limits of detection, reproducibility, linearity and selectivity was researched under the optimized conditions. As demonstrated in Fig. 6a, with increasing amount of Hg^{2+}, an obvious color change from gray purple to dark green and finally to navy took place. Fig. 6b further shows that with Hg^{2+} concentration increasing from 0 to 100 μmol/L, the LSPR band red-shifted and the intensity showed a regular increase trend at 550 nm, which can be ascribed to the gradual conversion of Ag_2S to HgS [35–37]. Fig. 6c shows that the variation of the peak intensity at 550 nm (ΔA_{550}) varied linearly with the concentration of Hg^{2+} and the equation is ΔA (550 nm) = 0.0041 × $C[Hg^{2+}]$ (μmol/L) + 0.0167 (R^2 = 0.9894). The limit of detection (LOD) is 1.21 μmol/L, calculated by the signal-to-noise of 3. The reproducibility of this method was validated by testing six replicates of standard solutions with Hg^{2+} concentration of 30.8 μmol/L, and the RSD was 0.12%.

To study the specificity of the proposed approach for Hg^{2+} detection, a number of anions and metal ions were detected under the parallel experimental conditions (Fig. 7). For the Hg^{2+} detection, the absorbance at 550 nm increased obviously with the color change from gray purple to dark green and finally to navy. While the addition of other compounds, even at the concentration of 25 to 1250 times of Hg^{2+}, cannot produce apparent spectral and color change. It is worth noting that $S_2O_3^{2-}$, I^- and Br^- have intensive coordination capability and usually corrode Ag with the aid of oxygen, so they may interfere with the detection. Nevertheless, the results show that Au/Ag_2S NPs exhibit a minimal response toward these ions, indicating this method has high selectivity and anti-interference ability. As mentioned before, such high selectivity is attributed to the extremely low solubility product of Ag_2S and low reactivity with those interferents. Compared to other reported nanoprobes for Hg^{2+} detection shown in Table S1 (Supporting information), the proposed method shows comparable sensitivity and linear response range, but has better selectivity and eliminates the needs for surface modification, making it viable in the direct analysis of Hg^{2+} in complex samples. To evaluate the viability of Au/Ag_2S NPs in natural water samples analysis, recovery tests were carried out for detecting tap water and sewage samples. As summarized in Table 1, the Hg^{2+} concentration in tap water was lower than the LOD of the approach, and the Hg^{2+} concentration in sewage samples was calculated as 15.40 μmol/L. The recoveries ranged from 100.5% to 102.8% and 93.1% to 97.3% in tap water and sewage samples, respectively, with RSDs in the range of 1.38%–2.89%, indicating the viability of the proposed method for Hg^{2+} in natural water samples. It should be emphasized that the sewage sample was directly analyzed without any sample pretreatment, indicating the high selectivity of the method.

To summarize, we proposed a rapid and highly specific colorimetric method for Hg^{2+} detection based on Au/Ag_2S dimeric NPs. We synthesized Au/Ag_2S dimeric nanoparticles *via* the epitaxial and lattice-mismatch process, which had an Au core with excellent optical properties and an Ag_2S portion with exclusive response towards Hg^{2+}. The sensing mechanism is attributed to the precipitation conversion of Ag_2S with Hg^{2+} to generate more stable HgS. This alters the components and structure of the nanoparticles, further causing the change of the LSPR effect, and the color and spectrum will also change accordingly. Due to the minimum solubility product of Ag_2S, Au/Ag_2S dimeric NPs have a minimal response to common interferents, so this method has high selectivity towards Hg^{2+}. Finally, the practicability of the method was validated by analyzing the raw sewage sample with satisfactory recoveries. This work not only provides a highly specific colorimetric method for on-site detection of Hg^{2+}, but also offers an insight to the design of specific plasmonic nanostructures as unique optical nanoprobes.

Declaration of competing interest

The authors declare no competing financial interest.

Acknowledgments

This work was supported by the National Natural Science Foundation of China (No. 21876206), the Key Fundamental Project of Shandong Natural Science Foundation (No. ZR2020ZD13), the Science and Technology Projects of Qingdao (No. 21–1–4-sf-7-nsh), and the Youth Innovation and Technology project of Universities in Shandong Province (No. 2020KJC007).

Supplementary materials

Supplementary material associated with this article can be found, in the online version, at doi:10.1016/j.cclet.2022.05.005.

References

[1] S. Liu, X. Wang, G. Guo, Z. Yan, J. Environ. Manag. 277 (2021) 111442.
[2] D.G. Streets, H.M. Horowitz, D.J. Jacob, et al., Environ. Sci. Technol. 51 (2017) 5969–5977.
[3] C.T. Driscoll, R.P. Mason, H.M. Chan, D.J. Jacob, N. Pirrone, Environ. Sci. Technol. 47 (2013) 4967–4983.
[4] T.W. Clarkson, L. Magos, G.J. Myers, New Engl. J. Med. 349 (2003) 1731–1737.
[5] K.H. Kim, E. Kabir, S.A. Jahan, J. Hazard. Mater. 306 (2016) 376–385.
[6] H. Erxleben, J. Ruzicka, Anal. Chem. 77 (2005) 5124–5128.
[7] Q. Niu, X. Wu, T. Li, et al., J. Fluoresc. 26 (2016) 1053–1058.
[8] J.V. Ros-Lis, M.D. Marcos, R. Mártinez-Máñez, K. Rurack, J. Soto, Angew. Chem. Int. Ed. 44 (2005) 4405–4407.
[9] Y. Tang, F. He, M. Yu, F. Feng, L. An, et al., Macromolecul. Rapid Commun. 27 (2006) 389–392.
[10] J.A. Moreton, H.Trevor Delves, J. Anal. Atom. Spectr. 13 (1998) 659–665.
[11] Z. Zhu, G.C.Y. Chan, S.J. Ray, X. Zhang, G.M. Hieftje, Anal. Chem. 80 (2008) 7043–7050.
[12] A. Piriya V.S, P. Joseph, K. Daniel, et al., Mater. Sci. Eng. C 78 (2017) 1231–1245.
[13] N. Ullah, M. Mansha, I. Khan, A. Qurashi, TrAC Trends Anal. Chem. 100 (2018) 155–166.
[14] B. Sepúlveda, P.C. Angelomé, L.M. Lechuga, L.M. Liz-Marzán, Nano Today 4 (2009) 244–251.
[15] D. Liu, W. Qu, W. Chen, et al., Anal. Chem. 82 (2010) 9606–9610.
[16] C.J. Yu, W.L. Tseng, Langmuir 24 (2008) 12717–12722.
[17] F. Chai, C. Wang, T. Wang, Z. Ma, Z. Su, Nanotechnology 21 (2009) 025501.
[18] C.W. Liu, Y.T. Hsieh, C.C. Huang, Z.H. Lin, H.T. Chang, Chem. Comm. (2008) 2242–2244.
[19] J.S. Lee, M.S. Han, C.A. Mirkin, Angew. Chem. Int. Ed. 46 (2007) 4093–4096.
[20] J.M. Slocik, J.S. Zabinski Jr, D.M. Phillips, R.R. Naik, Small 4 (2008) 548–551.
[21] J. Du, Y. Sun, L. Jiang, et al., Small 7 (2011) 1407–1411.
[22] Y. Guo, Z. Wang, W. Qu, H. Shao, X. Jiang, Biosens. Bioelectron. 26 (2011) 4064–4069.
[23] J. Yang, Y. Zhang, L. Zhang, et al., Chem. Commun. 53 (2017) 7477–7480.
[24] X. Chen, Y. Zu, H. Xie, A.M. Kemas, Z. Gao, Analyst 136 (2011) 1690–1696.
[25] G. Agrawal, R. Agrawal, ACS Appl. Nano Mater. 2 (2019) 1738–1757.
[26] T. Yang, L. Wei, L. Jing, et al., Angew. Chem. Int. Ed. 56 (2017) 8459–8463.
[27] P. Yánez-Sedeño, S. Campuzano, J.M. Pingarrón, Appl. Mater. Today 9 (2017) 276–288.
[28] J. Zeng, M. Li, A. Liu, et al., Adv. Funct. Mater. 28 (2018) 1800515.
[29] A.S.D.S. Indrasekara, B.J. Paladini, D.J. Naczynski, et al., Adv. Healthcare Mater. 2 (2013) 1370–1376.
[30] L. Rivas, S. Sanchez-Cortes, J.V. García-Ramos, G. Morcillo, Langmuir 16 (2000) 9722–9728.
[31] D.B. Pedersen, S. Wang, J. Phys. Chem. C 111 (2007) 1261–1267.
[32] J. Yang, J.Y. Ying, Chem. Commun. (2009) 3187–3189.
[33] B. Xiong, R. Zhou, J. Hao, et al., Nat. Comm. 4 (2013) 1708.
[34] G. Park, C. Lee, D. Seo, H. Song, Langmuir 28 (2012) 9003–9009.
[35] F. Zhang, L. Zeng, C. Yang, et al., Analyst 136 (2011) 2825–2830.
[36] S. Chen, J. Tang, Y. Kuang, et al., Sens. Actuator. B: Chem. 221 (2015) 1182–1187.
[37] L.M. Liz-Marzán, Langmuir 22 (2006) 32–41.